Polar Geosci., **18**, 1–14, 2005

Validation of grounding line of the East Antarctic Ice Sheet derived by ERS-1/2 interferometric SAR data

Tsutomu Yamanokuchi[1]*, Koichiro Doi[2] and Kazuo Shibuya[2]

[1]*SOKENDAI/Remote Sensing Technology Center of Japan, 12th Floor, Roppongi First Bldg., 1–9–9, Roppongi, Minato-ku, Tokyo 106-0032*
[2]*National Institute of Polar Research, Kaga 1-chome, Itabashi-ku, Tokyo 173-8515*
**Corresponding author. E-mail: tsutomuy@restec.or.jp*

(Received March 4, 2005; Accepted July 19, 2005)

Abstract: We applied Synthetic Aperture Radar (SAR) Interferometry (InSAR) in the East Antarctic marginal ice zone between 25°W and 40°E. ERS-1/2 tandem data received at Syowa Station in 1996 were mainly used. ERS interferograms with range-azimuth coordinates were transformed into World Geodetic System 1984 (WGS 84) coordinates. For this transform, we used the RAMP (RADARSAT Antarctic Mapping Project) image which is already defined by the WGS84 reference system. Significant features in the ERS intensity image show similar textures to those in the RAMP image. By taking the above features in the ERS intensity image as ground control points of known WGS84 geodetic coordinates from the RAMP image, we assigned WGS84 coordinate values to any element in the ERS scene by a least-squares fitting with a second-order polynomial function. It is noted that the ERS InSAR scene has the same WGS84 coordinate system as the ERS intensity scene. We extracted and digitized grounding lines from the ERS InSAR scene as a curve of steeply changing fringe pattern at the ocean-continent boundary. Features of the grounding line in the Antarctic Digital Database (ADD) were monotonous as interpreted from blurring of the Landsat image on the ice shelf and the ice sheet. In contrast, InSAR-derived grounding lines delineated complex features as a result of ocean tidal motion at the ocean-continent boundary. For example, the ADD shows a peninsula around 15°E, but it actually is a group of snow-covered islands or ice rises. The positional discrepancy of the ADD grounding line from the InSAR-derived grounding line reaches 5000 m around Riiser-Larsenhalvøya, and about 1200 m around Padda and Skallen.

key words: SAR, Interferometry, grounding line, ERS-1, ADD

1. Introduction

Behavior of the Antarctic ice sheet draws attention from the viewpoint of global environmental changes. Advance or retreat of the grounding line of the ice sheet is believed to be related to global environmental changes. Therefore, monitoring of the grounding line is important as an indicator of global environmental changes, although it is difficult to detect the grounding line by *in-situ* observations due to severe weather conditions in Antarctica.

Synthetic Aperture Radar (SAR) Interferometry (InSAR) is a microwave remote sensing technique developed in the early 1990's. It is well recognized now as a powerful tool for geographical and geophysical research in Antarctica. InSAR can acquire two-dimensional spatial information over a broad (more than 6400 km^2) inaccessible area at one time, and the observations are repeatable on a regular schedule. InSAR analysis uses a pair of SAR images observed in the same area on different dates, and detects the Earth's surface movement and topography by a fringe interferogram pattern. For example, Goldstein *et al*. (1993) applied InSAR to detect the grounding line at the Rutford Ice Stream, West Antarctica. In East Antarctica, Ozawa *et al*. (2002) applied this technique along the Prinsesse Ragnhild Kyst (Coast) to detect the grounding line and to estimate tidal motion in the ice-covered sea quantitatively.

The Scientific Committee on Antarctic Research (SCAR) has compiled a comprehensive geographical digital data base called the Antarctic Digital Database (ADD; ADD Consortium, 2000). The ADD has various kinds of geographic information and covers the whole Antarctic continent and its surrounding area. It is the only existing available data source for the grounding line in East Antarctica. However, the detailed positions and shapes have not been delineated in the ADD's grounding line data (hereafter, we describe these data as the 'ADD-GL' in this paper). Furthermore, Ozawa *et al*. (2002) pointed out the positional inaccuracy of the ADD-GL, up to several kilometers, along the Prinsesse Ragnhild Kyst.

In this study, we focused on the marginal ice zone between the East Antarctic continent and the ice shelves between 25°W and 40°E. We delineated the grounding lines along the 2000 km-long coastline in detail from InSAR and made a quantitatively more accurate map model than the ADD-GL model.

2. Procedure for comparison of InSAR derived grounding line with the ADD

In this section, we describe the procedure employed to compare the positions of grounding lines provided by ADD and InSAR. Details of used data sets will be described in the next section. InSAR images (interferograms) are generated from ERS-1 and ERS-2 (European Remote Sensing satellite 1 and 2) scenes, using a Gamma SAR signal processor (Gamma Remote Sensing, 2000) for both of the single look complex (slc) images and SAR intensity images. As detailed explanation of InSAR processing is given in Hanssen (2001), it is not repeated here.

The ADD-GL is expressed by the rectangular coordinates of the polar stereographic projection at the standard parallel of 71°S, and the World Geodetic System 1984 (WGS84) coordinates can be assigned to each position in the ADD-GL vector data base (ADD Consortium, 2000).

In case of ERS SAR intensity and InSAR scenes, only the four corners of the scene are assigned to WGS84 geodetic coordinates. As schematically illustrated in Fig. 1, the position of an element in the scene is specified by a combination of the pixel number i in the range direction and the line number j in the azimuth direction, where i varies from 1 to 2456 (2 look case) and j from 1 to typically 5000. The element has resolution of about 50 m in the azimuthal direction; that in the range direction is not uniform, but depends on the incident angle θ in Fig. 1.

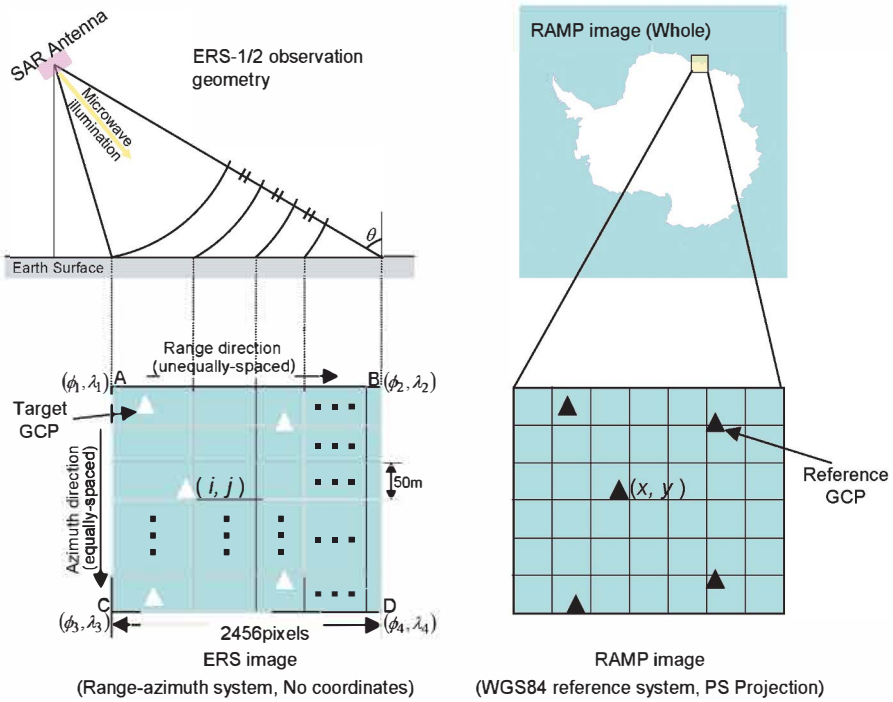

Fig. 1. Procedure to transform range-azimuth coordinates of the ERS intensity and InSAR scenes to the WGS84 geodetic coordinates is schematically illustrated. The location of the element in the ERS scenes is specified by a pixel number i in the range direction and the line number j in the azimuthal direction. The four corners (A, B, C, D) are assigned WGS84 coordinate values. We can assign WGS84 coordinate values of the RAMP GCPs (solid triangles on the right side) to the corresponding ERS GCPs (open triangles on the left side). A least-squares fitting with a second-order polynomial function defines the location of any ERS scene element in the WGS84 reference system.

In order to assign geodetic coordinate values to any element in the ERS SAR intensity scene, we take advantage of the existing SAR image data base made from RADARSAT (Canadian SAR satellite) observations, namely the RADARSAT Antarctic Mapping Project (RAMP) image data base by Jezek *et al*. (2002). Details of the RAMP image data base will be described in the next Section 3. What is important here is that the RAMP image data base is already characterized by polar stereographic coordinates in the WGS84 reference system.

As both ERS-1/ERS-2 and RADARSAT SAR use the same C-band (5.6 cm) radar wavelength, surface features in the ERS backscatter intensity images are quite similar to those in the RAMP image data base. Therefore, significant features in the ERS intensity image, that is, ground control points (GCPs), can be matched with the corresponding GCPs in the RAMP image data base. This in turn means that the WGS84 geodetic coordinates can be assigned to the GCPs in the ERS intensity image. A least squares fitting with a second-order polynomial function in the polar stereographic projection plane finally results in assigning WGS84 geodetic coordinate values to any

element in the ERS intensity image. We call this process "geometric correction". It is necessary to take at least 7 GCPs per image for this least squares fitting with a second-order polynomial function.

The image texture in the ERS interferogram is quite different from that in the ERS intensity image, but after geometric correction, element position in the ERS interferogram is the same as that of the corresponding element in the ERS intensity image. From this ERS interferogram, the grounding line can be detected and traced as a curve of steeply changing fringe pattern at the ocean-continent transition. We manually digitized this ERS interferogram derived grounding line (hereafter referred to as the 'InSAR-GL') by using PC-based digital Geographic Information System (GIS) software. Each position in the InSAR-GL vector data base is associated with the WGS84 geodetic coordinates.

3. Data used in this study

3.1. RADARSAT Antarctic Mapping Project SAR mosaic image (RAMP image)

In 1997, the whole Antarctic continent was observed by the Canadian SAR satellite RADARSAT-1 under the Antarctic Mapping Mission-1 (AMM-1) project. The RAMP AMM-1 SAR Image Mosaic of Antarctica version 2 (RAMP image) was produced in 2002 by the RADARSAT-1 Antarctic Mapping Project (RAMP) as a National Aeronautics and Space Administration (NASA) Pathfinder Project (Jezek *et al*., 2002). The RAMP image data set used in this study has 125 m spatial resolution and is projected in the polar stereographic coordinates of the WGS84 reference system. The standard parallel of this product is taken at 71°S. The RAMP image data set is available from both the Alaska Satellite Facility (ASF) and the National Snow and Ice Data Center (NSIDC). We take advantage here of the fact that the RADARSAT-1 satellite image already has geographical location information and this image can be used as a reference map for geometric correction of ERS interferograms. In this study, we used a subset of the 25°W–40°E region from the original RAMP image. The accuracy of geographical location in the RAMP image reference map is estimated as $\pm$200 m according to Jezek (2002).

3.2. Grounding line data in the ADD

In the ADD, grounding line and coastline data are provided as vector data in ESRI ARC/INFO export file format, where ESRI and ARC/INFO are trademarks of Environmental Systems Research Institute, Inc., Redlands, CA, USA. These data are given in polar stereographic coordinates in the WGS84 reference system with a standard parallel at 71°S. According to the explanatory text of the ADD (ADD Consortium, 2000), the ADD-GL data in our study area were generated by interpretation of Landsat satellite optical images, and positional accuracy of the coastline is not specified as it varies depending on the region.

3.3. ERS-1 and ERS-2 SAR data for detecting grounding line

The ERS-1 and ERS-2 SAR data used in this study are summarized in Table 1. The numbers in column 1 correspond to the image numbers in Fig. 2; they are located

Table 1. ERS-1/ERS-2 data.

No.	Observation date	Observation mode	Receiving station	Baseline perpendicular distance (Bp)	No. of GCPs
1	1999/11/14-15	Tandem	Syowa	151	8
2	1991/12/06-09	Ice mode	Syowa	69	8
3	1996/04/02-03	Tandem	Syowa	29	8
4	1996/04/11-12	Tandem	Syowa	76	9
5	1996/04/17-18	Tandem	Syowa	17	8
6	1996/05/28-29	Tandem	Syowa	71	8
7	1996/04/03-04	Tandem	Syowa	64	7
8	1996/06/02-03	Tandem	Syowa	69	7
9	1996//05/21-22	Tandem	Syowa	37	9
10	1996/04/03-04	Tandem	Syowa	12	9
11	1996/04/05-06	Tandem	Syowa	76	7
12	1996/04/05-06	Tandem	Syowa	76	7
13	1996/04/11-12	Tandem	Syowa	14	7
14	1996/05/08-09	Tandem	Syowa	59	10
15	1996/04/09-10	Tandem	Syowa	43	7
16	1996/06/02-03	Tandem	Syowa	7	7
17	1996/04/02-03	Tandem	Syowa	36	7
18	1996/03/17-18	Tandem	O'Higgins	127	8
19	1996/03/07-08	Tandem	O'Higgins	168	8
20	1995/11/07-08	Tandem	O'Higgins	27	7
21	1997/03/14-15	Tandem	O'Higgins	74	7
22	1995/11/13-14	Tandem	O'Higgins	94	9
23	1996/02/29-03/01	Tandem	O'Higgins	117	7
24	1996/04/09-10	Tandem	Syowa	10	22
25	1996/02/18-19	Tandem	Syowa	190	9
26	1995/11/08-09	Tandem	O'Higgins	138	8
27	1996/04/18-19	Tandem	Syowa	70	9

Pairs of ERS SAR data for interferometry. Numbers in column 1 corresponds to image numbers in Fig. 2. Column 2 is observation date of a pair of InSAR images, column 3 is observation mode, and column 4 is name of ERS data receiving station. Column 5 is baseline perpendicular distance, and the last column is the number of GCPs used for geometric correction.

from 40°E west to 25°W. The acquisition dates of the SAR pairs (column 2) range mostly from November 1995 through June 1996. This period was during the "SAR Tandem Mission over Antarctica" which was planned by the European Space Agency

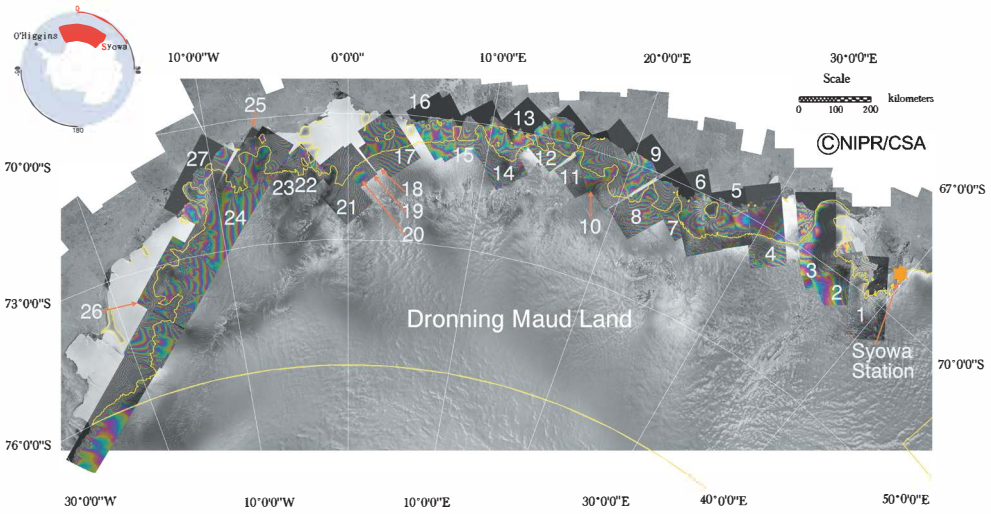

Fig. 2. Analyzed area in this study. The number on each interferogram corresponds to that in column 1 in Table 1. The orange star indicates the location of Syowa Station. Yellow lines indicate the coast line and grounding line drawn from the Antarctic Digital Database (ADD Consortium, 2000).

(ESA). Data acquired during this mission period are labeled "Tandem" in column 3, which means that ERS-2 followed 1 day after ERS-1 and observed the same scene with a time delay of 1 day. The tandem pair of images No. 1 in 1999 were acquired by special order from the National Institute of Polar Research (NIPR). No. 2 scenes were acquired during December 1991 of ERS-1 "Ice Mode" under the commissioning phase with a repeat time span of 3 days. As compared with usual ERS satellites' repeat observation time span (35 days), short repeat time span such as Tandem (1 day) or Ice mode (3 days) is suitable for observations over the Antarctic ice sheet because it can avoid temporal decorrelation (Hanssen, 2001).

Column 4 indicates the receiving station; "Syowa" indicates that data were received by the 11 m Syowa multipurpose satellite antenna (Hirasawa *et al.*, 1990). The "Syowa" data were converted from the RAW tape format to the common satellite data format using the SAR data processing system of NIPR (Doi *et al.*, 2000). "O'Higgins" indicates the German satellite receiving antenna at the Chilean O'Higgins Station located on the Antarctic Peninsula; data received by that antenna were purchased from ESA.

As compared with JERS-1, the satellite orbits of both ERS-1 and ERS-2 were controlled precisely to follow the same orbit as repeatably as possible. The baseline perpendicular distance Bp in column 5 means the orthogonal component of baseline distance between two related ERS orbits with respect to the ground target. For the selection of appropriate scene pairs, satellite orbit data of shorter Bp is preferable. Longer Bp causes decorrelation of the interferogram; the critical baseline distance to maintain a good interferogram is less than approximately 1060 m in the case of ERS-1/2 SAR (Zebker *et al.*, 1994). All Bp values in column 5 of Table 1 were shorter than 200 m; baseline conditions of all the selected ERS data pairs in Table 1 fulfilled the

condition of Zebker *et al*. (1994).

When we calculate the baseline distance, we adopted the ERS-1/ERS-2 satellite orbit data provided by the Delft Institute for Earth-oriented Space Research (Delft-orbit; Scharroo and Visser, 1998) instead of the original orbit data. The Delft-orbit was calculated with supplemental information such as Radar Altimeter (RA) data and Satellite Laser Ranging (SLR) data, and is known to be more accurate than the original predicted orbit data.

Column 6 shows the number of GCPs for geometric correction between the ERS images and the RAMP image. The number of GCPs is at least 7 per pair; 227 GCPs are used for the geometric correction.

4. Comparison of InSAR-GL with ADD-GL

After the coordinate transform described in Section 2, the ERS interferograms and the InSAR-GL are described by the WGS84 geodetic coordinate system, similarly to the RAMP image data base and the ADD-GL. Therefore it is possible to overlay the InSAR-GL onto the RAMP image data base by taking it as a reference. We overlaid all of the 27 InSAR interferograms onto the RAMP image data base as illustrated in Fig. 2. The yellow line shows the ADD-GL and some portion of the coastline, which is also drawn onto the RAMP image data base. As for the InSAR-GL, we will look into Fig. 2 for 3 typical regions from east to west and discuss their characteristic features.

4.1. Features between 20°E and 40°E

The red line in Fig. 3 shows the InSAR-GL, while the blue line shows the grounding line obtained by interpreting the SAR intensity image. Around the Shirase Hyôga (Glacier), the InSAR-GL and the ADD-GL showed good consistency with detailed features. Many intensive observations and ground surveys have been done by the Japanese Antarctic Research Expeditions (JAREs) around 38°E–40°E, and their results are reflected in the ADD. However, we can see a conspicuous positional difference between the InSAR-GL and the ADD-GL around Padda (69°39′S, 38°20′E) and Skallen (69°40′S, 39°25′E). The InSAR-GL lies approximately 1200 m westward from the ADD-GL.

From Fig. 3, the InSAR-GL around Shirase Hyôga can be identified clearly as 16 km inland from the ADD-GL, and 12 km wide as compared with the 9 km wide ADD-GL. Therefore, we investigated if temporal changes in the Shirase Hyôga's grounding line had occurred recently. The position of the grounding line was completely the same between 1996 (Fig. 4a) and 1999 (Fig. 4b) within the spatial resolution (50 m) of the interferogram. Drastic changes of glacial ice did not occur during this period, and we interpret the above difference as having resulted from inaccurate position data in the ADD-GL.

As Ozawa *et al*. (2002) pointed out, disagreement in the spatial positions of grounding lines between the InSAR-GL and the ADD-GL becomes significant around the northern tip of the Riiser-Larsenhalvøya (Peninsula); it attained approximately 5000 m (Fig. 5).

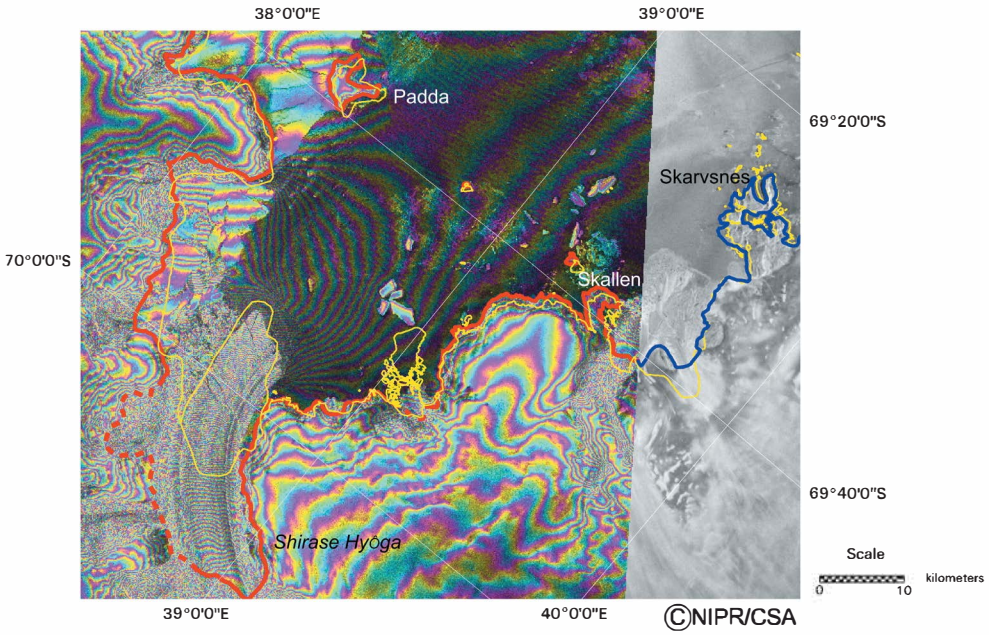

Fig. 3. Overlaid image of grounding line and interferograms around the Shirase Hyôga. Yellow lines indicate the ADD-GL. Red lines indicate the InSAR-GL, where the dotted portion indicates the region of lower-confidence. The blue line is the grounding line and coast line derived from the SAR intensity image.

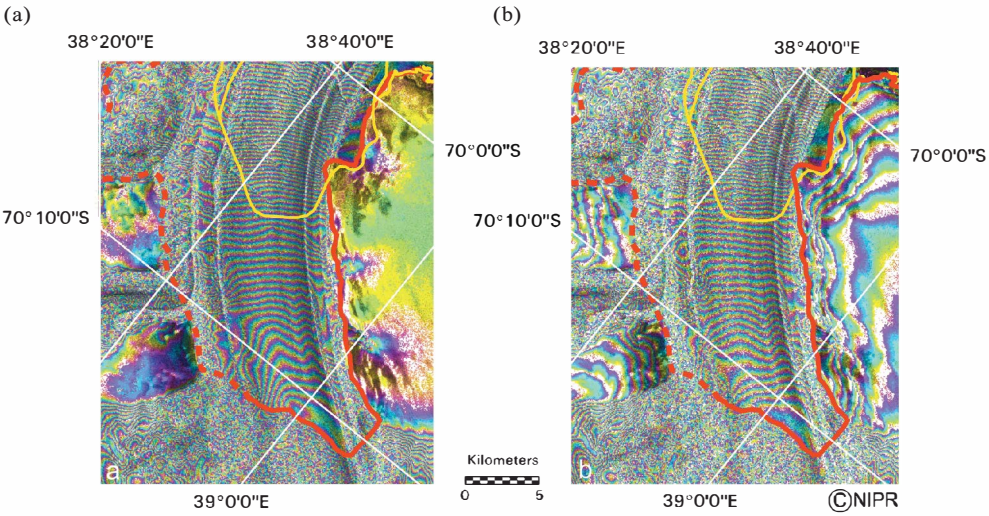

Fig. 4. Enlarged interferograms around the grounding line of the Shirase Hyôga. The left side (a) was observed in June 1996 and the right side (b) was observed in November 1999. The color code of grounding lines is the same as in Fig. 3.

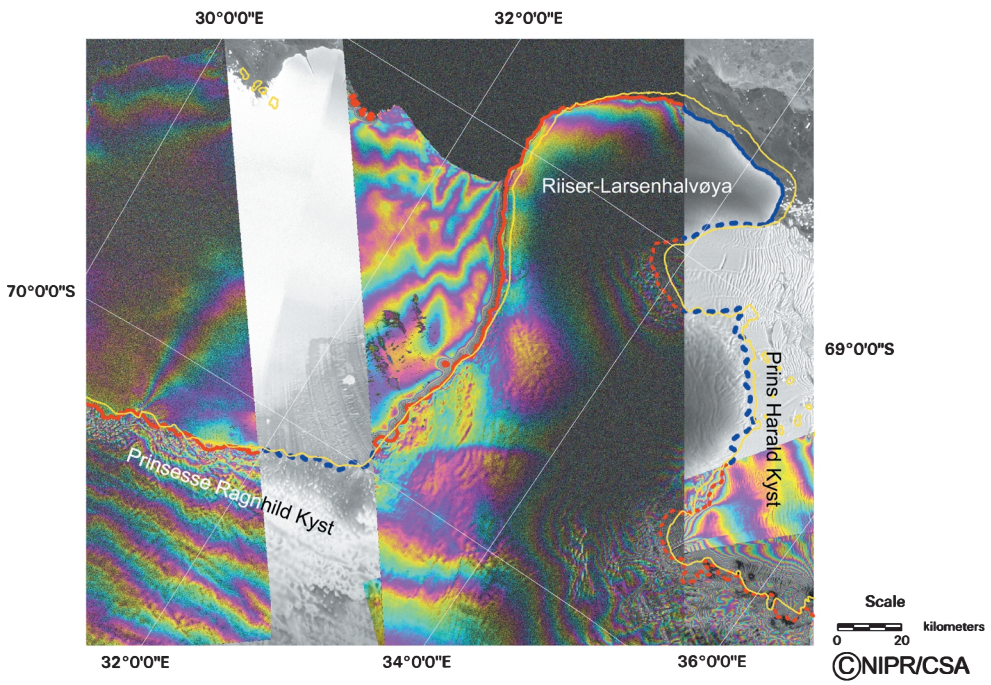

Fig. 5. Overlaid image of grounding line and interferograms around the Riiser-Larsenhalvøya. Yellow lines show the ADD-GL. Red lines show the InSAR-GL, while the blue line is that derived from the SAR intensity image. The dotted portion indicates the region of lower-confidence.

4.2. Features between 0° and 20°E

Figure 6a shows grounding lines around Lazarevisen (13°E–16°E). The yellow ADD-GL lost most of the detailed features in this area, and became monotonous showing an erroneous peninsula-like grounding line. In contrast to the ADD-GL, detailed shapes are delineated in the red InSAR-GL. Actually, there is no peninsula in this region; the false pattern in the ADD-GL must be generated by amalgamation of three isolated islands or ice rises. This may be due to the fact that the ADD-GL was interpreted from Landsat satellite images (Near-infrared and visible optical sensors) and no *in-situ* observation results were used in this region (ADD Consortium, 2000).

Figure 6b shows an intensity image from ERS-1 SAR. It is very difficult to interpret the grounding line from this image. In addition, two islands or ice rises that are not catalogued in the ADD can be found from the InSAR-GL about 60 km north of the continental grounding line. These two objects (69°47′S, 13°13′E and 69°43′S, 13°40′E) are enclosed by green circles in Fig. 6 and Fig. 7, where Fig. 7 is the overlay of SAR intensity images acquired in 1992 and 1997. Cyan color shows the ERS-1 SAR image acquired in 1992, while red color shows the RADARSAT-1 image acquired in 1997. From Fig. 7, the locations and shapes of these two objects are found to be unchanged for more than 5 years, although other marginal ice shelves changed. Therefore, we interpret them as snow-covered islands or ice rises. These two islands may pin-tie the ice

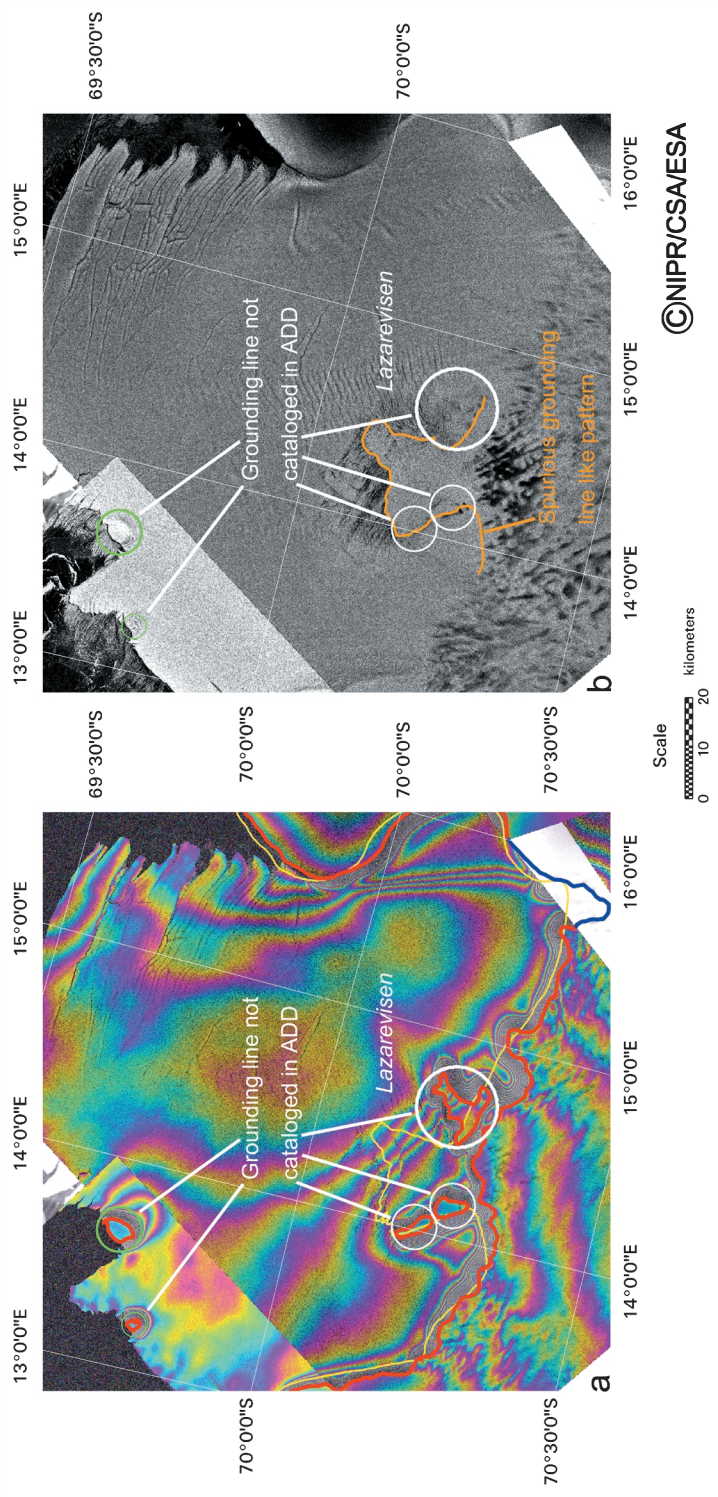

Fig. 6. (a) Overlaid image of grounding line and interferograms around Lazarevisen, and (b) ERS-1 intensity image of the same area. The color code is the same as before (Fig. 5).

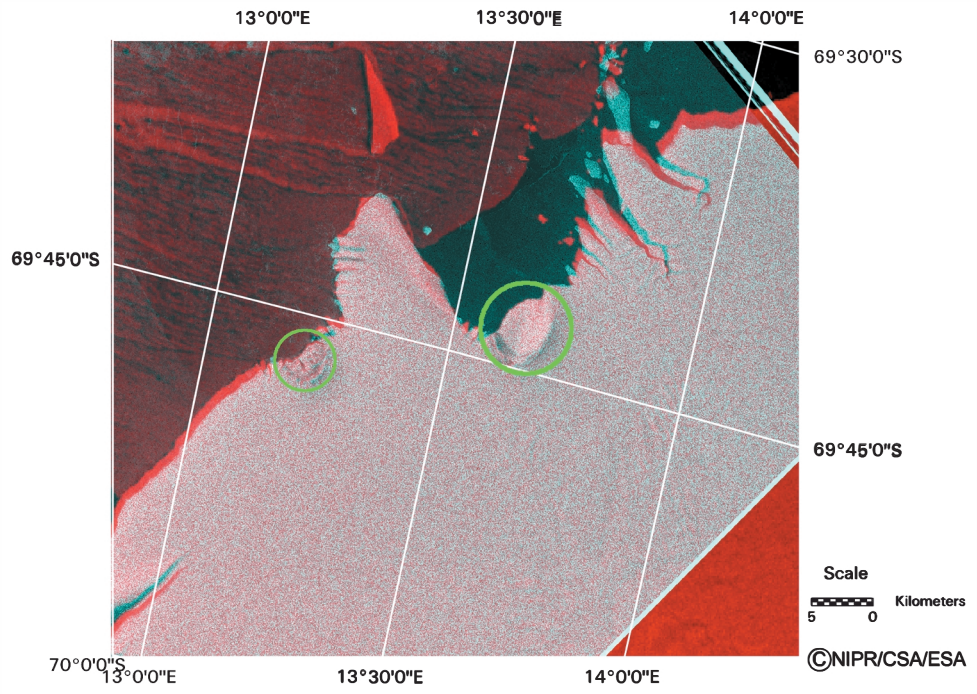

Fig. 7. Overlay of SAR intensity images. Cyan color shows the ERS-1 SAR intensity image acquired in 1992 and red color shows the RADARSAT-1 SAR intensity image acquired in 1997.

shelves of Lazarevisen and may play an important role in stabilizing the sea-ice mass balance of this region.

In summary, detailed shapes of the InSAR-GL are quite different from those of the ADD-GL in this region, though the geographical locations of both grounding lines roughly coincided.

4.3. Features between 0° and 20°W

This area showed complex configuration in the ERS-1 intensity image as shown by Fig. 8a. Several glaciers, small islands, and hill-like features overlay intricately in one area. Around Robertskollen, it is difficult to trace the grounding line from the interferogram, as indicated by the dotted portion in Fig. 8b. The InSAR-GL on Jutulstraumen (glacier around 1°W) is located approximately 43 km south of the ADD-GL, as in the Shirase Hyôga region.

Interferometric fringes in the coastal marginal ice zone usually consist of three components, that is, topographic fringe, fringe caused by tidal motion (grounding line), and fringe due to glacial flow. If tidal motion of the ice shelf is small, it becomes difficult to detect the grounding line. Since the estimated vertical tidal displacement from the NAO99b ocean tide model (Matsumoto *et al.*, 2000) between the two SAR scenes around Robertskollen is only 9.4 cm, it is not sufficient to detect the grounding line features clearly. Furthermore, glacial flows also make the fringe pattern ambigu-

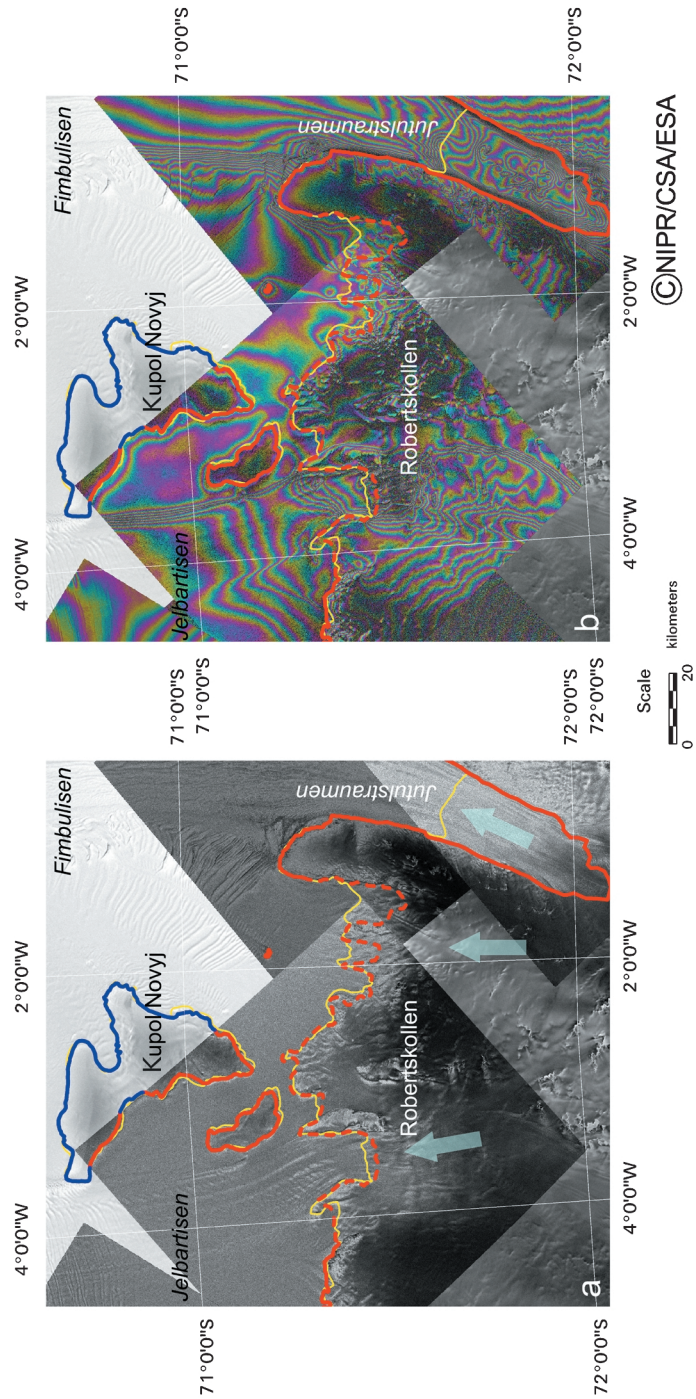

Fig. 8. (a) ERS-1 intensity image around Robertskollen, where light blue arrows indicate glaciers and (b) overlaid image of grounding line and interferograms in the same area. The color code is the same as before (Figs. 5–6).

ous. Because the estimated ocean tide amplitude from the NAO99b model approximately attains 1 m per day on other days, there may be other appropriate InSAR pairs for clear detection of grounding lines.

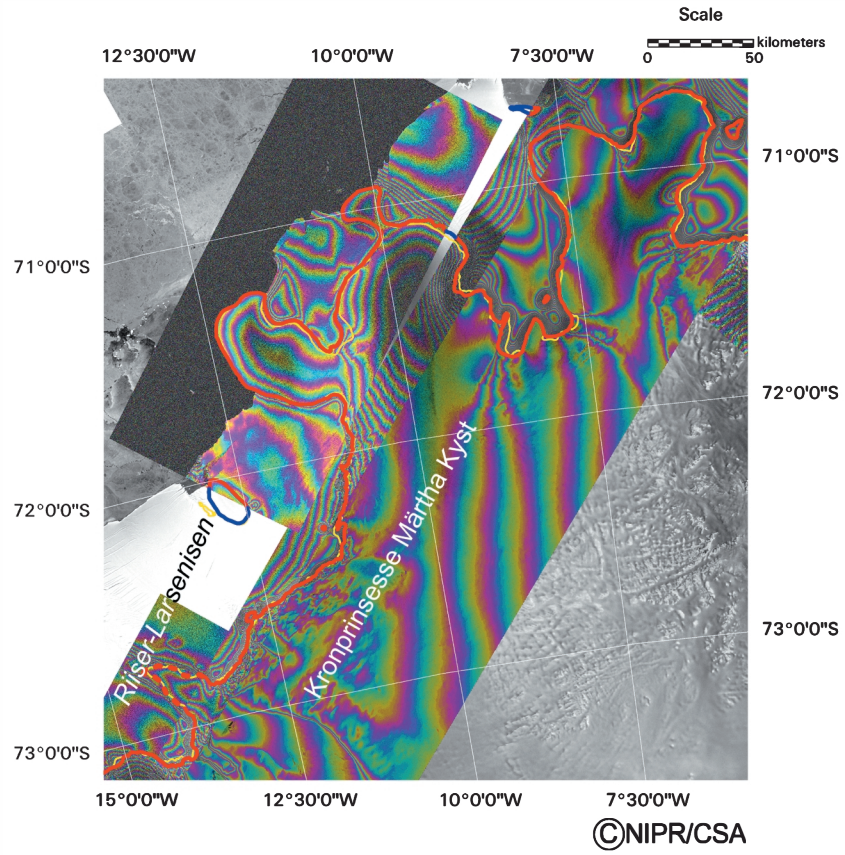

Fig. 9. Overlaid image of grounding line and interferograms along the Kronprinsesse Märtha Kyst. The color code is the same as before (Figs. 5–6, 8).

Figure 9 shows grounding lines along the Kronprinsesse Märtha Kyst. As compared with the previous areas, features of the InSAR-GL match those of the ADD-GL. This good correspondence continues toward the west end of Riiser-Larsenisen.

5. Conclusions

We have presented precise grounding lines of the East Antarctic continent between 25°W and 40°E obtained by an InSAR analysis, and provided their position data in a general GIS vector data format. This region has the longest marginal ice zones in East Antarctica, and spaceborne SAR is the most appropriate means to extract geographical location and shapes of the grounding line in detail.

Geographical location of the InSAR-GL is roughly consistent with the ADD-GL

except for Padda, Skallen, and Riiser-Larsenhalvøya. However, the InSAR-GL delineated extremely detailed features except around 0° as compared with the monotonous ADD-GL. The InSAR-GL in the glacier is located inland as compared with the ADD-GL; for example, 16 km inland beneath the Shirase Hyôga and 43 km inland beneath Jutulstraumen. Around Robertskollen, it was difficult to interpret grounding lines from the interferogram because of the vague fringe pattern. This may be due to the small tidal motion.

Acknowledgments

The ERS-1/2 data used in this study were acquired at Syowa Station by the JARE satellite receiving team, except for No. 18–23 and 26. The ERS-1/2 data acquired at Syowa Station were partially produced and provided by the Japan Aerospace Exploration Agency/Earth Observation Center. The authors are grateful to their contribution to the data production. We especially express sincere thanks to JARE-37 for their extensive reception of the SAR Tandem Mission over Antarctica. We also would like to thank two anonymous referees for critical reading of the manuscript.

References

ADD Consortium (2000): Antarctic Digital Database, Version 3.0. Database, manual and bibliography. Cambridge, Scientific Committee on Antarctic Research, 93 p.

Doi, K., Ozawa, T., Aoki, S., Shibuya, K. and Oishi, Y. (2000): Level 0 CEOS formatted data generating system for SAR data of NIPR. Proc. Workshop "SAR interferometry and its application", ed. by N. Fujii. Tokyo, Earthquake Remote Sensing Frontier Project, on CD-ROM.

Goldstein, R.M., Engelhardt, H., Kamb, B. and Frolich, R.M. (1993): Satellite radar interferometry for monitoring ice sheet motion: Application to an Antarctic ice stream. Science, **262**, 1525–1530.

Gamma Remote Sensing (2000): Gamma Modular SAR Processor (MSP) Reference Manual.

Hanssen, R.M. (2001): Radar Interferometry. Dordrecht, Kluwer, 308 p.

Hirasawa, T., Ejiri, M., Inada, T., Ohasi, S., Endo, K., Kuzuya, R., Okamoto, H., Nagao, T., Sato, S. and Chiba, M. (1990): Multipurpose satellite data receiving system. NEC Tech. Note, **43** (4), 73–94 (in Japanese).

Jezek, K. (2002): RADARSAT-1 Antarctic Mapping Project: change-detection and surface velocity campaign. Ann. Glaciol., **34**, 263–268.

Jezek, K. and RAMP Product Team (2002): RAMP AMM-1 SAR Image Mosaic of Antarctica. Alaska Satellite Facility, Fairbanks, AK, in association with the National Snow and Ice Data Center, Boulder, CO. Digital media.

Matsumoto, K., Takanezawa, T. and Ooe, M. (2000): Ocean tide models developed by assimilating TOPEX/POSEIDON altimeter data into hydrodynamical model: A global model and a regional model around Japan. J. Oceanogr., **56**, 567–581.

Ozawa, T., Shibuya, K., Doi, K. and Aoki, S. (2002): Detection of grounding line and vertical displacement of ice shelf by SAR interferometry. Polar Geosci., **15**, 112–122.

Scharroo, R. and Visser, P.N.A.M. (1998): Precise orbit determination and gravity field improvement for the ERS satellites. J. Geophys. Res., **103**, 8113–8127.

Zebker, H.A., Werner, C.L., Rosen, P.A. and Hensley, S. (1994): Accuracy of topographic maps derived from ERS-1 interferometric radar. IEEE Trans. Geosci. Remote Sensing, **32**, 823–836.